JOURNAL OF MECHANICAL ENGINEERING AND SCIENCES
ISSN: 2289-4659 e-ISSN: 2231-8380
VOLUME 18, ISSUE 4, 2024, 10247 - 10260
DOI: https://doi.org/10.15282/jmes.18.4.2024.3.0809

UNIVERSITI MALAYSIA PAHANG AL-SULTAN ABDULLAH

RESEARCH ARTICLE

Numerical and hydrodynamic analysis of a container vessel due to the change of collision wave angle at different speeds in regular wave

M. Mokhtari[1], S. Jamei[1], Z. Razaviyan[1], M. Heidari[2], S. Thangavel[2], A. Kumar[3,4]*

[1] Faculty of Engineering, Persian Gulf University, Boushehr, 7516913817, Iran
[2] Department of Mechanical Engineering, Global College of Engineering and Technology, P.O. Box 2546 CPO Ruwi 112, Muscat, Sultanate of Oman
[3] Department of Mechanical Engineering, Technical Education Department Uttar Pradesh, Kanpur 208024, India
[4] Department of Mechanical Engineering, Grahic Era deemed to be University Dehradun 248002, Uttarakhand, India

ABSTRACT - This study investigates the dynamic behavior of a container ship subjected to different Froude numbers and collision angles. The primary focus is on the ship's vertical motion, torsion, roll, and resistance under varying sea conditions. The generated wave height and wave formation resistance significantly increase by increasing the Froude number and the ship's speed in calm water. The second quarter of the ship encounters the wave bottom at an altitude of 0.065290 meters, followed by a lighter blue hue at an altitude of 0.032864 meters. The vertical motion function at different wave angles (0°, 30°, 60°, 90°, 120°, 150°, 180°) and the total resistance coefficient at various collision angles were analyzed. The findings reveal a substantial increase in dynamic movements and additional resistance due to wave-induced motion as the Froude number rises. The maximum extra resistance occurs when the wave impacts the ship's bow. The calculated conversion functions for torsional and vertical motions closely align with existing laboratory results, demonstrating an error of less than 10%, which is acceptable for numerical simulations. These findings are crucial for understanding and mitigating the challenges faced by ships operating in various sea conditions.

ARTICLE HISTORY
Received : 31st Jan. 2024
Revised : 09th July 2024
Accepted : 06th Sept. 2024
Published : 30th Dec. 2024

KEYWORDS
Computational fluid dynamics
Dynamic movements
Resistance
Container ship
Froude numbers
Turbulence model
Navier-Stokes equations

1. INTRODUCTION

The efficient movement of ships through water is crucial for economic and environmental reasons. However, navigating open seas presents significant challenges due to the impact of waves, currents, and wind. These factors contribute to 'added resistance' a force that significantly reduces a vessel's speed compared to calm water conditions. Studies suggest that added resistance can account for 15-30% of a ship's total resistance [1]. This additional force is critical in ship design, particularly propulsion systems. Accurately predicting added resistance ensures sufficient power to maintain desired speeds while minimizing fuel consumption and emissions. The primary source of added resistance arises from wave interaction with the ship's hull. Research indicates that the magnitude of this resistance depends heavily on several factors, including the ship type, hull shape, and environmental conditions experienced during operation [2]. Ship designers, therefore, face the challenge of optimizing hull design to minimize wave resistance. Understanding the relationship between hull geometry and resistance is crucial in achieving this goal. Traditionally, the two main methods for estimating added resistance are analytical and experimental. Laboratory experiments involve testing a scaled model ship in a controlled environment. Initially, the model's resistance is measured in calm water. Next, the model is subjected to regular or irregular waves, typically replicating head-on wave encounters at a constant design speed. Finally, added resistance is calculated by comparing the average resistance measured under wave conditions to the calm water resistance at the same speed.

In the analytical method, the mathematical model of ship motion in the wave is extracted and solved by numerical methods, and as a result, the additional resistance is calculated. Understanding the behavior of a ship on a real sea route is very important in characterizing its performance. Rough sea conditions cause severe movements in the ship, and this affects the ship's resistance. Increased resistance may affect effectiveness and raise fuel consumption. Ship movements and maritime behavior are very important for the safety of the crew, the ship, and the cargo. It is important to be aware of the effects of ship movement on resistance. Many of the existing techniques for predicting ship motion and the increased resistance because of waves depend on assumptions derived from potential flow theory, including free-surface impacts. On the other side, most previous investigations, such as Schmitke [2], demonstrate that the impacts of viscosity are the most important effects, especially in large amplitude waves and large Froude numbers. According to Beck and Reed [3], the early 21st century saw strip theory dominate maritime calculations, accounting for roughly 80% of all analyses. This popularity stemmed from its speed and applicability to the geometry of most container ships. However, limitations emerged as ship speeds and wavelengths increased. Newman [4] identified inaccuracies in conventional strip theories when dealing with long waves and high Froude numbers. These errors stemmed from the simplified treatment of forward motion and the complex nature of wave scattering around the ship. Similarly, Faltinsen and Zhao [5] argued that strip

***CORRESPONDING AUTHOR | A. Kumar** | ✉ drashwanikumardte@gmail.com

theory loses accuracy at high speeds due to its rudimentary approach to forward velocity. These limitations fuelled the exploration of more advanced methods. Three-dimensional approaches, such as the Rankin panel method and the mean time method, gained traction alongside advanced computational fluid dynamics (CFD) techniques like Reynolds-Averaged Navier-Stokes (RANS) and Large Eddy Simulation (LES). As computing power became more accessible, the application of these three-dimensional methods to maritime problems grew significantly. Yasukawa and Bertman [6] emphasized the emergence of these methods as a response to the shortcomings of strip theory. Unlike strip theory, three-dimensional methods consider the full impact of flow velocity and forward motion, leading to more accurate calculations for high-speed vessels and complex hull shapes.

Yasukawa and Bertman [6] used the concept for several high-velocity container vessels. The findings of this investigation revealed that the hydrodynamic forces, ship movements, and local pressures using Yasukawa and Bertman [6] theory were much better predictions than the experimental band theory results. However, the estimated lateral hydrodynamic forces are inadequate due to the viscosity effect. Yasukawa [7] suggested that the issue could be resolved by using experimental corrections similar to those used in the tape concept. Simonsen et al. [8] emphasized that impacts overlooked in potential concepts, like brittle waves, turbulence, and viscosity, should be considered immediately in numerical methods. RANS procedures, for example, are excellent alternatives to potential flow theory because they can immediately incorporate viscosity impacts into their equations [8]. Continuous technical developments have significantly increased computing power. Therefore, it can be used for viscous flow simulations to solve RANS equations in the time domain. With the improvement of technology, computational fluid dynamics RANS methods quickly became popular in marine functions. These ways have a distinct benefit and allow designers to access the ship's performance at sea during the design process, thus allowing for complete remedial action before the ship is built [9]. As stated by Simonsen et al. [8], many researchers have widely applied RANS-based CFD approaches to analyze maritime performance on several types of ships. CFD simulations were also performed for ships with more complex geometric shapes. Carrica et al. [10] proved one application of the unstable RANS CFD (URANS) method in simulating ship deflection for the Office of Naval Research (ONR) tumblehome with automatic guidance in both regular and irregular forward waves. Then, Castiglione et al. [11] examined the motor reactions of a high-speed DELFT catamaran at regular forward waves at three different velocities. Castiglione et al. [12] conducted CFD simulations to investigate the navigation of the same ship design at two different Froude numbers, considering both regular and oblique forward waves. Simonsen and Stern [13] conducted CFD RANS simulations to achieve torsional and vertical motions, added strength for the KCS design, and presented it at the Gutenberg CFD workshop [13]. In this study, it was shown that CFD outcomes are consistent with experimental results [14].

Kim [15] performed CFD analyses for a 6,500 container carrier centering on overall ship movements and structural loads with successful validation of results based on design test measurements. After accreditation studies, Kim stated that the current state of CFD technology would make ship optimization decision-making easier [15]. Figures 1 and 2 show the three-dimensional view of the body of the container vessels, the side view and the deck. Figure 3 shows the water line surface deck. Maruo [16] developed calculations for additional resistance by determining the transverse and longitudinal components of the second-order horizontal average wave force acting on a ship in regular waves. He employed the laws of momentum, energy, and potential flow theory to achieve this. Utilizing the direct pressure integration method, Goodman [17] calculated the average vertical force of the second order exerted on a submerged cylinder. The cylinder was examined in regular waves from front to side for wavelengths equal to the diameter of the cylinder. In this regard, no comparison was made between the laboratory and the obtained results [17]. Momentum theory and relationships proposed by Maruo [16], in addition to the second-order horizontal force, Newman [18] also calculated the second-order vertical moment for a desired object, and in particular, a lean vessel in regular waves. Gerritsma and Beuckelmann [19] calculated the extra resistance on the 60 Series models using potential theory and the direct pressure integration method. Faltinsen et al. [20] calculated the additional strength of a ship. They also proposed a simplified formula for calculating the extra resistance at short wavelengths, which well modeled the interference between reflected waves and uniform current around the ship [20]. Pinkster et al. [21] calculated second-order forces and moments using the direct method of direct pressure integration at different frequencies. Tezdogan et al. [22] studied the resistance of a full-scale KCS ship by using RANS-based CFD to reduce fuel consumption and economic requirements.

The previous studies concluded that ship design, particularly propulsion selection, heavily relies on minimizing wave resistance, a significant component of total resistance. Additional wave resistance, influenced by environmental conditions, needs to be considered [23-25]. Real-world scenarios involve measuring this resistance in laboratories (calm water against regular/irregular waves) or using analytical methods (solving a mathematical model of ship motion in waves). Both approaches aim to calculate the difference in resistance compared to calm water conditions. Current prediction techniques often rely on assumptions from potential flow theory, neglecting viscosity effects [26-30]. Matulja et al. [28] have studied the wave-induced resistance and noted three main effects: 1) Drifting force: interaction between incoming waves and ship-generated waves due to vertical and torsional motions; 2) Scattering force: interference between waves and the ship hull, significant for short wavelengths relative to ship length, 3) Damping force: vertical and torsional motions in calm water. Accurate prediction of these forces is crucial for calculating total resistance, emphasizing the need for precise motion and response calculations. Vertical displacement and longitudinal vessel movements significantly affect the extra resistance. When the ship's movements are small, the additional resistance due to the scattering of the waves at high wave frequencies prevails. This is due to the small movements of the ship due to the impact waves, and the

ratio of the incoming wavelength to the length of the ship is low. However, the impact waves will be reflected from the ship. When the ship's movements are large, the extra resistance due to the radiation of the dominant waves occurs, which occurs in the resonance zone of the vertical movements and the vessel torsion [28]. However, recent studies emphasize the importance of viscosity, especially at high wave amplitudes and Froude numbers. While strip theory remains popular due to its speed and applicability to container ships, limitations arise for high-velocity vessels and complex hull shapes. This has led to the developing of more advanced three-dimensional methods like the Rankin panel method and CFD techniques like RANS and LES [31-34]. Unlike strip theory, these methods account for the full impact of flow velocity and forward motion. Additionally, the increasing computing power allows for solving complex fluid dynamics simulations using RANS equations. This has led to the widespread adoption of CFD-RANS methods in maritime applications, as evidenced by various studies simulating ship behavior and resistance in different wave conditions [35-37].

The main objective of this study is to investigate the dynamic behavior of a container ship under varying Froude numbers using the κ-ε method with a 1:31.6 scale model. Unlike Tezdogan et al. [22] employed a full-scale model with two degrees of freedom at specific speeds, this analysis considers five Froude numbers and different speeds for head-on wave collision. Additionally, this article examines the ship's behavior at seven wave impact angles with three degrees of freedom (vertical motion, torsion, roll), comparing both motion responses and resulting added resistance.

2. MATERIALS AND METHODS

The Korean Container Ship (KCS) model, which is attached to the rudder with scale, was used in this study. The major features of the KCS design are listed in Table 1 [15]. The service speed for this ship is set to 24 knots. According to Simonsen's experiments, waves with different Froude numbers and characteristics were selected for more detailed examination in the validation study. Table 2 shows the wave properties used for the study. Figures 4 and 5 depict the computational field for the ship simulations, focusing on the right half of the hull due to symmetry. Boundary conditions are also presented in these figures. Wave scattering (interaction of waves and hull) and wave dumping (vertical and torsional movements) are important factors considered in the analysis. The shape of the vessel geometry and its characteristics and side views are shown in Figures 1-3. To avoid border crossings, selecting the type and placement of borders is crucial. Figure 1 illustrates the chosen border types, while Figure 2 depicts their positions in the area's front and side views. The characteristics of the vessel and the conditions of the waves are stated in Tables 1, 2, and 3, and the boundary conditions are shown in Figures 4 and 5. All the calculations in the STAR-CCM + have been done in these initial conditions.

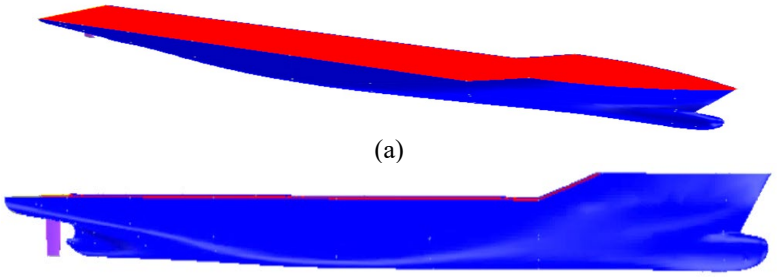

(a)

(b)

Figure 1. (a) 3D model of a container vessel and (b) Side view of a container vessel

Figure 2. View of the upper deck of the container

Figure 3. Water line surface vessel

Table 1. KCS vessel specifications

Parameters	Values
Space between columns, L_{BP}	7.2700 m
Waterline length, L_{WL}	7.3500 m
Water line beam, B_{WL}	1.0100 m
Depth, D	0.6000 m
Displacement, Δ	0.0016 m
Block factor, C_B	0.6505 m

Table 2. Waves applied in computational fluid dynamics software

Froude no, F_n	Wave height, H	Ship Length / Wavelength $\frac{\lambda}{L_{BP}}$	Wave slope, $\frac{H}{\lambda}$	Collision frequency, F_e	Wavelength, λ
0.178					
0.205					
0.232	0.14	8.37	0.69	1.6	1.15
0.260					
0.287					

In this study, a standard turbulence model that is frequently used in industrial applications was employed. Querard et al. [23] also mentioned that the model uses a lot less central processing unit (CPU) time than the Shear-stress transport (SST) turbulence model, wherein 25% more CPU time is required. To simulate the realistic behavior of the ship, the dynamic fluid hull interaction model (DFBI) was used with a ship that freely performs up and down and torsional movements. The DFBI design enables the RANS solver to calculate the moments and excitatory forces acting on the hull due to the waves and to solve the equations of motion of the governing rigid body to regenerate the rigid body [24]. Figure 4 shows the overview of the computational range in the KCS body model and the concepts of the selected boundary conditions. Only half of the hull (right side of the ship) is displayed to minimise the need and computational complexity. A plane of symmetry forms the face of the central domain so that the other half of the design is accurately simulated. It should be noted that the symmetry condition is applied only in the case of wave collision from the bow and stern, and in other angles, symmetry is not used.

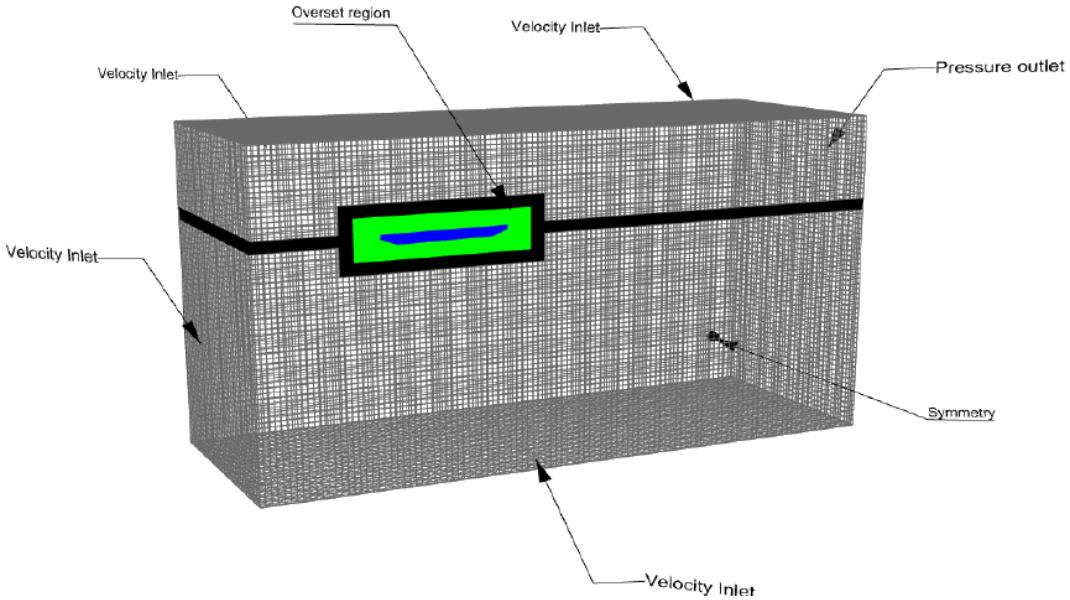

Figure 4. Overview of boundary conditions

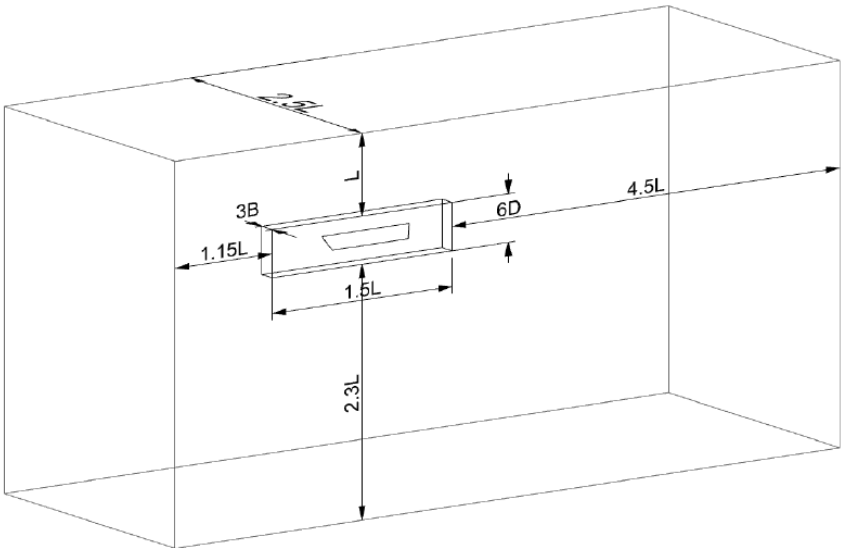

Figure 5. Computational field dimensions for marine simulations

Figures 4 to 5 depict the boundary conditions used for the simulation. Speed inputs generate regular forward waves on the positive x-axis, while pressure output is modeled on the negative side. Velocity inlets at the top and bottom prevent fluid-wall interaction and represent deep water with open ventilation. Pressure outlet at the rear stabilizes the flow. These choices, informed by Star-CCM+ studies [24], minimize boundary effects on the flow around the hull [25]. Alterskjær et al. [26] devise that for simulations in the presence of waves, the input limit of 1 to $2L_{BP}$ should be away from the body, while the output should be 3 to 4 L_{BP} below the current level to prevent the wave from returning from the wall. The calculation of conversion functions is important to define ship motions. The zero-harmonic amplitude, φ_0 in frequency spectrum (FS) is defined as the average amount of time data, $\varphi(t)$,that can be obtained as follows:

$$\varphi_0 = \frac{1}{T}\int_0^T \varphi(t)dt \tag{1}$$

The first FSφ_1 harmonic is a linear expression derived from unstable temporal data. Hence, the zero and first harmonicas of FS are called the principal components in the linear system. Previous research by Shen and Wan [27] on zero- and one-order expressions for force and motion was utilized in this study. These expressions were the basis for calculating resistance and conversion functions (TF). Conversion functions can quantify ship motions among waves. The definition of torsional and upward conversion and vertical motion functions are as follows:

$$TF_3 = \frac{x_{31}}{\xi_1} \tag{2}$$

$$TF_4 = \frac{x_{41}}{k\xi_1} \tag{3}$$

$$TF_5 = \frac{x_{51}}{k\xi_1} \tag{4}$$

The data for vertical motion, roll, torsion, and incoming waves, in the order of their first harmonic amplitudes in the Fourier series, are represented by x_{31}, x_{41}, x_{51}, and ξ_1, respectively, and $k = 2\pi/\lambda$ is the wave number. The total resistance of a vessel was investigated in both wave and calm water conditions using the dimensionless total resistance coefficient, C_T and is calculated as follows:

$$C_T = \frac{F_X}{\left(\frac{1}{2}\right)\rho U^2 S} \tag{4}$$

In this regard, F_X is the force *X* measured in the main coordinate system (total resistance) and *S* is the soaked surface of the ship in calm water. The increased resistance because of the waves was calculated by subtracting the calm water resistance $F_{X,calm}$from the harmonic amplitude of the Fourier series *X*-force between the waves ($F_{X,wave}$) at the same velocity of the ship. This value was dimensioned as follows:

$$\sigma_{aw} = \frac{(F_{X,wave} - F_{X,calm})}{\rho g \xi_{I1}^2 B_{WL}^2/L_{BP}} \tag{5}$$

where, σ_{aw} is the added resistance coefficient.

3. RESULTS AND DISCUSSION

3.1 Calculation of Additional Resistance at Different Froude Numbers

The extensive amount of data available for the KCS dataset provides a valuable resource for validating the accuracy of computational simulations. By comparing simulation results with experimental data, researchers can gain confidence in the methods and outcomes of their models. Table 3 details the characteristics of specific wave conditions (Simonsen waves) investigated in a laboratory setting. These wave characteristics, such as wave height and wavelength, are crucial for replicating realistic sea states within the simulations. Table 4 serves as a key comparison point, presenting the conversion functions for torsional and vertical ship motions obtained from the current CFD model alongside the experimental results documented by Simonsen et al. [8]. Additionally, the table compares the total resistance coefficient calculated by the model with the available experimental data. The inclusion of a comparison error in Table 4 provides further insight.

Table 3. Wave characteristics

Items	Speed (knot)	Wave height (m)	Wavelength (m)	Wave amplitude (m)	Wave slope	Ship Length /Wavelength
1		0.1228	8.3702	0.07000		1.15
2	24	0.1418	9.6890	0.08080	1.60	1.33
3		0.0191	14.5572	0.01216		2.00

Table 4. Comparison of conversion functions with Simonsen results

No.	Wave Model	TF_3	TF_5	C_T
1	Experimental Fluid Dynamics [8]	0.95	0.693	5.133×10^{-3}
	The current CFD	0.902	0.62	5.08×10^{-3}
	Error (%)	- 5.01	-9.3	-1.1
2	Experimental Fluid Dynamics [8]	1.107	0.971	5.843×10^{-3}
	The current CFD	1.002	0.873	5.71×10^{-3}
	Error (%)	- 9.44	- 10	- 2.26
3	Experimental Fluid Dynamics [8]	0.901	1.037	4.146×10^{-3}
	The current CFD	0.81	1	4.17×10^{-3}
	Error (%)	- 9.54	- 2.67	0.52

The comparison of the outcomes demonstrates that the results for the conversion functions of torsional and vertical motions were matched with the existing laboratory results, and it was observed that the resulting error is less than ten per cent, which is acceptable for numerical calculations. Also, the total resistance coefficient was compared with the available laboratory results, which showed that the results of the numerical solution are very close to the laboratory results. Less than three per cent error was obtained, indicating the accuracy of the numerical results. The waveform pattern around the vessel body and the wave condition of the collision with the float were recorded in all respects, which are the results in Figures 6 to 9. Based on the wave characteristics in Table 2, the wave pattern has a wavelength of 8.37 meters, a frequency of 0.069 Hz, and a height of 0.14 meters. This wave pattern is applied in controlled conditions where the vessel is fixed and only the wave on the ship.

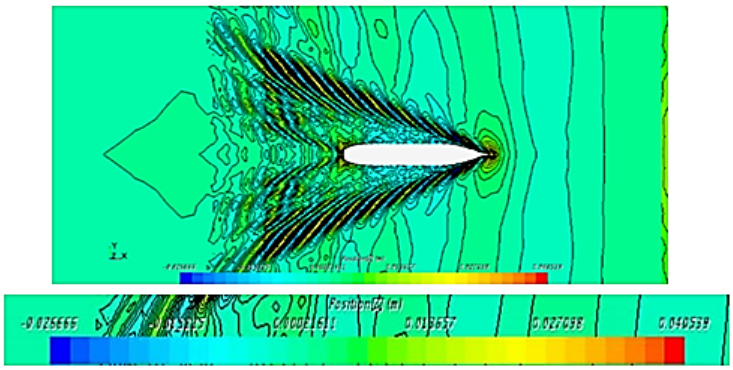

Figure 6. Wave pattern and wave height around the vessel body at Froude number 0.205 in calm water

Figure 6 depicts the wave pattern generated by the ship in calm water. This dominant wave is pale blue and has an average height of approximately 0.0002 meters. Here, the wave height varies considerably along the ship's length. The peak near the bow reaches a height of 0.0405 meters, while the lowest point at the stern dips to -0.0257 meters.

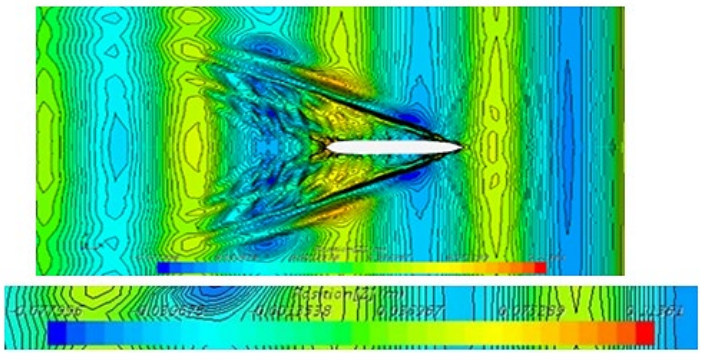

Figure 7. Wave pattern and wave height around the vessel body at Froude number 0.205 in dealing with waves

Figure 7 depicts the initial wave pattern encountered by the vessel. These waves are characterized by a light blue colour and an average height of approximately -0.00135 meters and focus on the interaction between these waves and the ship hull. It presents the resulting wave heights around the vessel at six key locations. The impact of the ship's geometry on the wave pattern is significant. The interaction creates a more complex wave profile than the initial waves. The highest point occurs at the floating bow, reaching a height of 0.11361 meters. This indicates a positive interference between the initial wave and the vessel's presence. Across the front half of the vessel's side, the colour spectrum in the figure suggests wave heights ranging from -0.0013538 meters to -0.039673 meters (light blue spectrum). This implies minimal negative

interference between this region's wave and hull. In the stern (back) of the vessel, the colour spectrum transitions to green and yellow. These colours indicate a rise in wave height, likely due to constructive interference between the wave and the ship's hull. This part experiences heights between 0.073289 meters and 0.036967 meters. In continuation, the colour spectrum shifts back to orange and red at the vessel's stern. This signifies another increase in wave height, potentially reaching a maximum positive interference of 0.11361 meters.

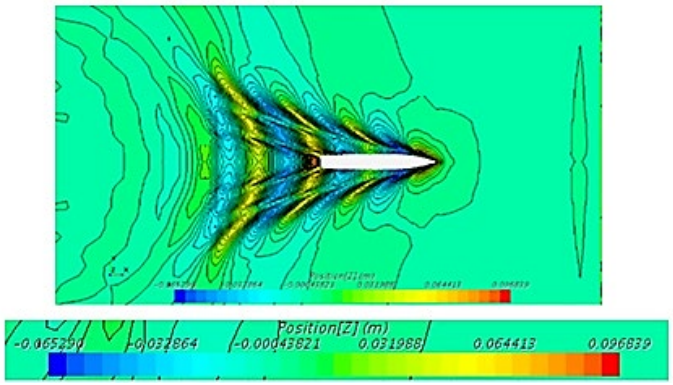

Figure 8. Wave pattern and wave height around vessel body at Froude number 0.26 in calm water collision

Figure 8(a) depicts the wave pattern around the ship in calm water (Froude number 0.26). The dominant colour, indicating the wave height, is pale blue. This calmness changes as the Froude number increases due to the corresponding rise in buoyancy velocity. The wave height peaks at six points along the ship's length, ranging from 0.096839 meters at the bow to -0.065290 meters at the bottom. While these values suggest a calm overall state, the wave pattern deviates from a perfectly flat surface due to the ship's hull geometry and increasing velocity, particularly at the bow. This observation aligns with the expected outcome: as Froude number and ship speed rise in calm water, the generated wave height increases. This, in turn, leads to higher wave resistance, impacting the ship's overall performance.

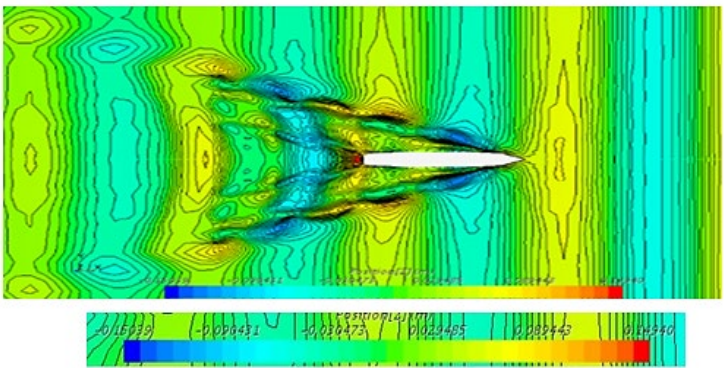

Figure 9. Wave pattern and wave height around the vessel body at Froude number 0.26 in collision with waves

Figure 9 depicts the wave pattern generated by the ship at a low Froude number of 0.026 in calm water. As the Froude number (ship speed) increases, the wave pattern and wave height change significantly compared to lower speeds. The highest wave peak reaches 0.115 meters, while the lowest point dips to -0.904 meters. Despite the influence of the applied wave on the overall pattern, the increased speed (higher Froude number) alters the gentle wave pattern observed at lower speeds. The colour spectrum of the ship in Figure 9(b) indicates that a significant portion (between 0.089 and 0.029 meters) experiences a shallow wave zone (yellow and green). The bow section encounters a deeper wave region (light blue) at the bottom, reaching depths between -0.305 and -0.904 meters. However, most of the ship's length remains in the positive wave height zone (yellow, orange, and red). These observations suggest that with increasing Froude number (speed), the wetted surface area of the ship increases due to its interaction with the waves. This can directly lead to higher resistance. Additionally, the figure implies a decrease in the wave breaking angle at the stern as the Froude number increases. This phenomenon might be related to the larger ship motions observed in Figures 10 and 11 (presented for vertical and torsional motions at different Froude numbers). Large ship movements can induce additional resistance due to wave radiation, particularly when the wave frequency coincides with the ship's natural frequencies of vertical and torsional motions (resonance zone) [28]. Table 2 summarizes the characteristics of the applied wave used in the simulations. The wave has a wavelength of 8.37 meters, a frequency of 0.069 Hz, and a height of 0.14 meters. This wave pattern is relevant for studying the unfixed ship's behavior, where the ship can respond freely to wave-induced motions.

Figures 6 to 9 illustrate the wave patterns around the vessel in calm water and during wave collisions at Froude numbers 0.205 and 0.26. These figures show a clear relationship between Froude number and wave behavior. As the Froude number increases, so do the ship's oscillations. This larger movement can lead to a higher wetted surface area on the hull, consequently increasing the overall resistance. Additionally, the figures show a decrease in the wave refraction

angle at the vessel's stern with increasing Froude number. This observation aligns with theoretical expectations and supports the validity of the simulations. The analysis proceeded in two steps to isolate the effect of the Froude number. First, the vessel was analyzed in calm water conditions to establish a movement baseline. This data provided a reference point for understanding how wave interaction affects the ship's behavior. Subsequently, the impact of wave (characteristics listed in Table 2) on the ship was investigated at five different Froude numbers. The results of this analysis are presented in Figures 10 and 11 for two specific cases.

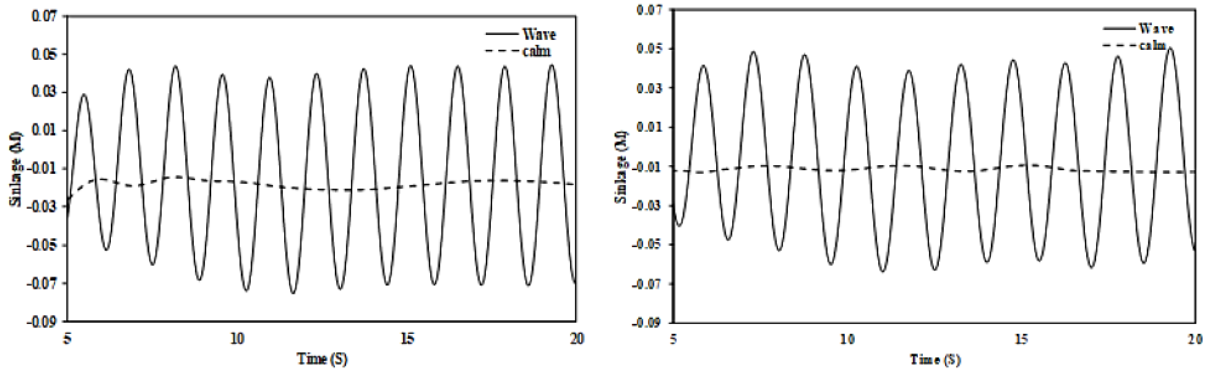

(a) (b)

Figure 10. Vertical motion diagram: (a) Froude number 0.205 and (b) Froude number 0.26

Figure 10(a) depicts the vertical motion of the container ship at a Froude number of 0.205. The motion can be visualized as a sine wave with values ranging from 0.7 (peak) to -0.9 (trough). This translates to a wave height of approximately 0.51 meters at the peak and 0.68 meters at the bottom over 20 seconds. Notably, the wave generated by the ship at this Froude number is relatively low. Similarly, Figure 10(b) illustrates the vertical motion at a Froude number of 0.26. The wave motion again resembles a sine wave with a peak of 0.7 meters and a trough of -0.9 meters. The key observation here is the difference in the initial wave behavior compared to Figure 10(a). At Froude number 0.26, the initial movement (positive) appears to push the wave upwards, contributing to the peak formation. In contrast, the initial movement at Froude number 0.205 (negative) seems to counteract the wave formation, pushing it downwards.

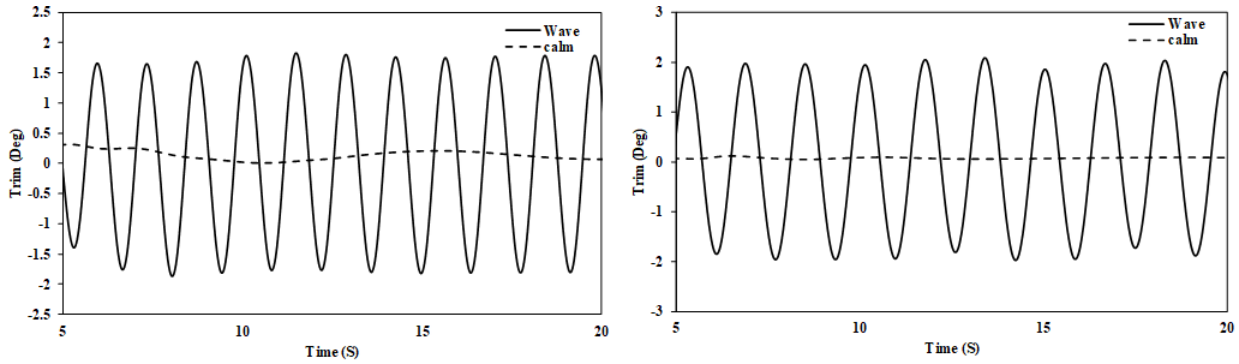

(a) (b)

Figure 11. Diagram of torsional motion: (a) Froude number 0.205 and (b) Froude number 0.26

Figure 11 depicts the vertical motion of the ship at different Froude numbers. The ship has no vertical motion in calm water (dashed line). However, in wavy water (sinusoidal line), the ship exhibits vertical and rotational movements. At a Froude number of 0.205 (Figure 11(a)), the wave height oscillates between a maximum of 1.8 units and a minimum of -1.8 units, with a period of 20 seconds. This indicates a larger range of vertical motion compared to higher Froude numbers. Additionally, the wave has more peaks and troughs, suggesting a slower oscillation frequency. At a Froude number of 0.26 (Figure 11(b)), the wave height oscillates with a smaller amplitude compared to Figure 11(a). The peaks and troughs are closer together, indicating a higher oscillation frequency. These observations suggest that wave characteristics change with the Froude number. The results from the numerical simulations are used to calculate conversion functions for torsional and vertical motions, as well as the total resistance coefficient and additional resistance for different Froude numbers. These results are presented in Figures 12 to 13. Table 2 details the wave specifications used in the simulations, designed to induce rotational motion in the vessel. The numerical solutions were then employed to calculate the conversion functions for both torsional and vertical motions. Additionally, the total resistance coefficient and the additional resistance experienced by the ship at various Froude numbers were determined. The results of these calculations are presented in Figures 12 and 13 for further analysis.

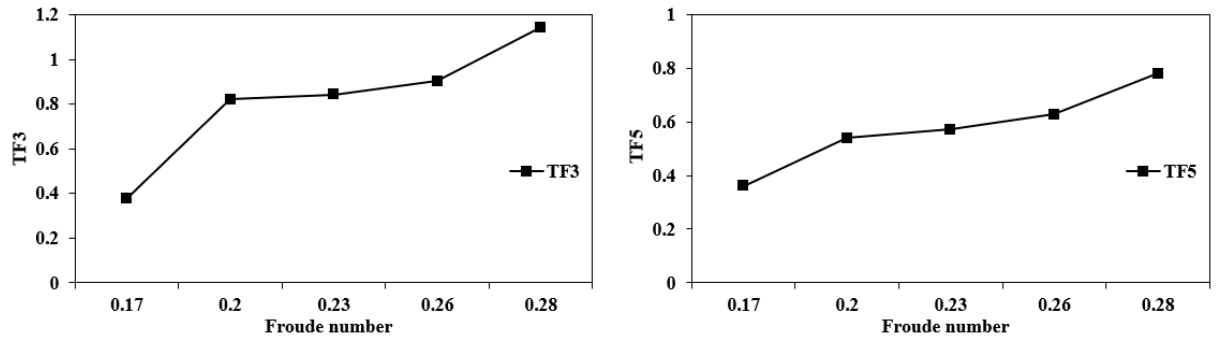

(a) (b)

Figure 12. Conversion functions of floating motions in different Froude numbers: (a) Torsional motion and (b) Vertical motion

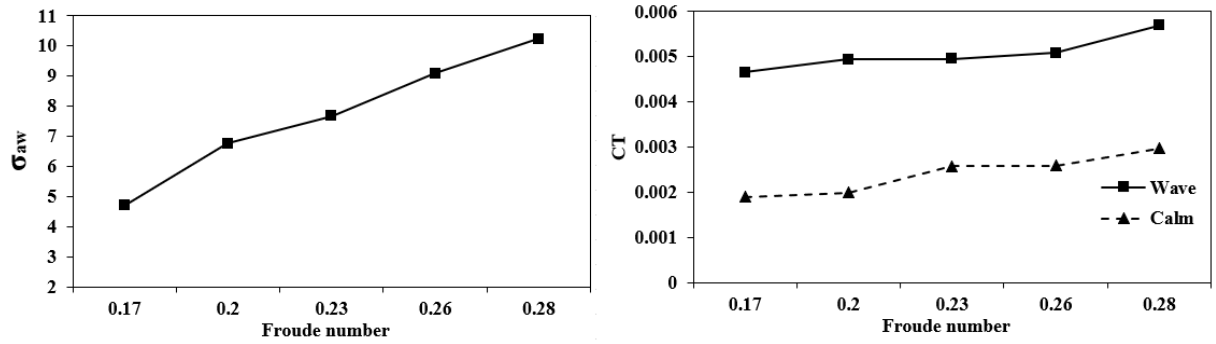

(a) (b)

Figure 13. The effect of increasing the Froude number on (a) additional resistance and (b) the total resistance coefficient

Figure 12 highlights a significant impact of Froude number on ship motions. As the Froude number increases from 0.17 to 0.28, the vertical and torsional motion conversion functions nearly triple and double, respectively. These results suggest that higher Froude numbers dramatically increase ship fluctuations and buoyancy variations. Consequently, fuel consumption rises significantly. Furthermore, neglecting these dynamic motions during ship design can endanger the vessel, cargo, and crew. The numerical solutions directly correlate with increasing Froude number and amplified buoyancy motions. This translates to a rise in both the buoyant force acting on the ship and the additional wave resistance it experiences. Figure 8 visually confirms this trend. At a Froude number of 0.28, the maximum wave resistance reaches 10.22, whereas it's only 4.68 at a Froude number of 0.17.

Figure 13(b) explores the relationship between the Froude number and the ship's total resistance coefficient in calm water and regular waves. It demonstrates that the coefficient increases for both calm water (dashed line) and regular waves (solid line) as the Froude number (indicating ship speed) increases from 0.17 to 0.28. This trend confirms that higher speeds lead to greater overall resistance. Furthermore, Figure 13(a) analyses the influence of the Froude number on the additional resistance coefficient caused by the ship's waves. Similar to the total resistance, the additional resistance also exhibits a rising trend with increasing Froude number, as shown by the values ranging from 0.688109 to 10.2286. This aligns with the findings presented in Equations 4 and 5. A rise in Froude number correlates with increased floating movements, contributing to higher forces acting on the ship and, ultimately, greater wave resistance. This is evident in Figure 13, where the maximum wave resistance of 10.22 occurs at the highest Froude number of 0.28.

3.2 Calculation of Additional Resistance at Different Collision Angles

Since the angle at which waves strike a ship at sea is often unpredictable, it is crucial to understand the ship's behavior under various wave impact angles. It is important to note that the results presented in this section are specific to regular waves, whose characteristics are detailed in Table 5. The simulations were conducted with waves striking the vessel at seven distinct angles to comprehensively analyse the effects of wave impact from different directions. Figure 14 shows a schematic diagram of the wave interaction with the ship at various angles.

Table 5. Wave characteristics at 0.17 Froude number

Froude number	Wave height (m)	Wavelength (m)	Wave amplitude (m)	Wave slope	Ship Length / Wavelength
0.17	0.1228	8.3702	0.07	1.60	1.15

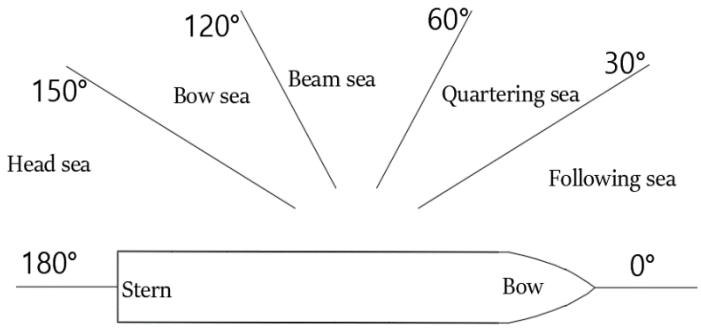

Figure 14. Different angles of waves colliding with the vessel [3]

This section investigated the effects of collision waves on a container ship at various angles relative to its float (main hull). The angles considered, as defined by Beck and Reed [3], were 0° (head-on collision), 30°, 60°, 120°, 150°, and 180° (following seas). The analysis focused on roll, torsion, and vertical displacement for specific wave collision angles to optimise computational efficiency. Due to the ship's symmetrical hull and minimal roll influence from bow and stern waves, only twisting and vertical motions were evaluated for these specific angles (0° and 180°). For all other wave collision angles (30°, 60°, 120°, and 150°), the range of ship roll motion was also included in the analysis. Figures 15 to 19 show the results of the vertical motion function, roll motion conversion function, torsion motion conversion function, total resistance coefficient and added resistance coefficient at different wave angles.

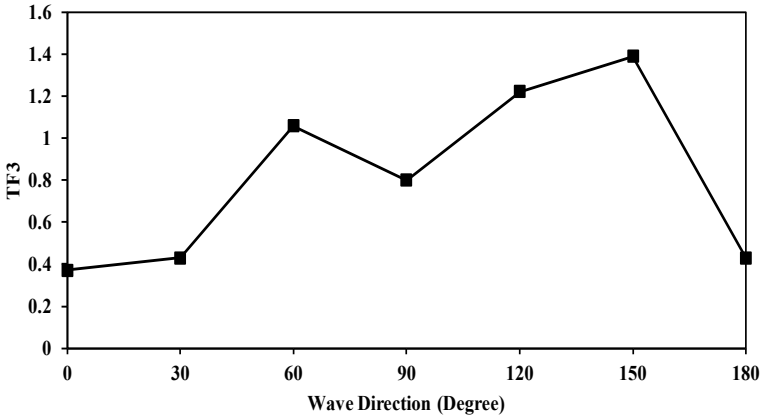

Figure 15. Vertical motion function at different wave angles

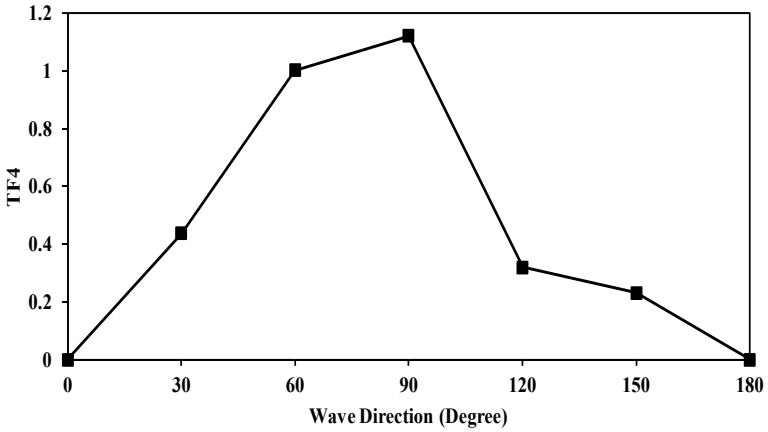

Figure 16. Roll motion conversion function at different wave angles

The impact of wave collision angle on the ship's dynamic motions is visualized in Figures 15 to 17. Figure 15 shows the vertical motion function at different angles of the wave at angles 0°, 30°, 60°, 90°, 120°, 150°, and 180° in the direction of 0.371376 and 0.431367, 1.05842, 0.799886, 0.799886, 1.390758, 0.42851, while Figure 16 shows roll motion conversion function at different wave collision angles in the direction 0.361528, 0.761112, 1.119406, 0.824213 and -0.30445, respectively. The 0.57872 and -0.55004 have the highest values at an angle of 90° degrees. Figure 15 depicts the vertical motion response function at various wave angles. It reveals that the vertical motion is most significant when waves approach from a specific angle (around 150 degrees). Similarly, Figure 16 shows the roll motion response function across different collision angles. The analysis indicates that the maximum roll motion occurs when waves strike the ship from the side (around 90 degrees). This is because wave interaction exerts a significant twisting force on the ship, causing

it to roll. Figure 17 explores the torsional motion response function. It suggests that the torsional deflection of the ship is most prominent at a particular angle (around 60 degrees) when waves collide with the vessel. Figures 15 to 17 clearly correlate wave collision angle and the ship's dynamic behavior. The vertical motion is most pronounced at a specific angle of 150 degrees, while roll motion is most severe when waves hit the ship from the side or at an angle of ninety degrees. Additionally, the torsional deflection reaches its peak at 60 degrees.

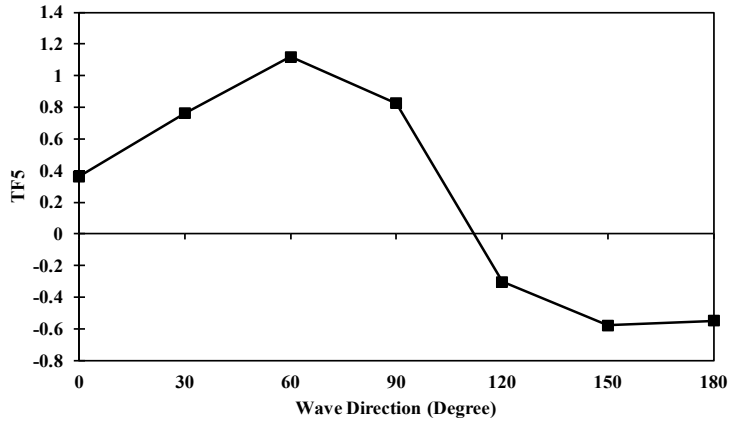

Figure 17. Torsion motion conversion function at different wave collision angles

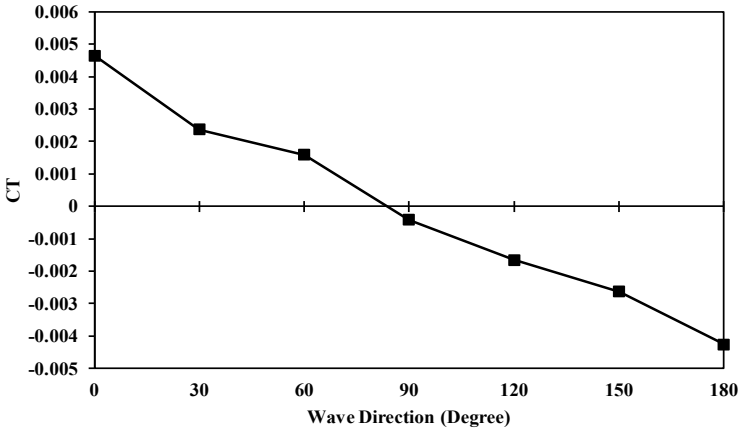

Figure 18. Total resistance coefficient at different wave collision angles

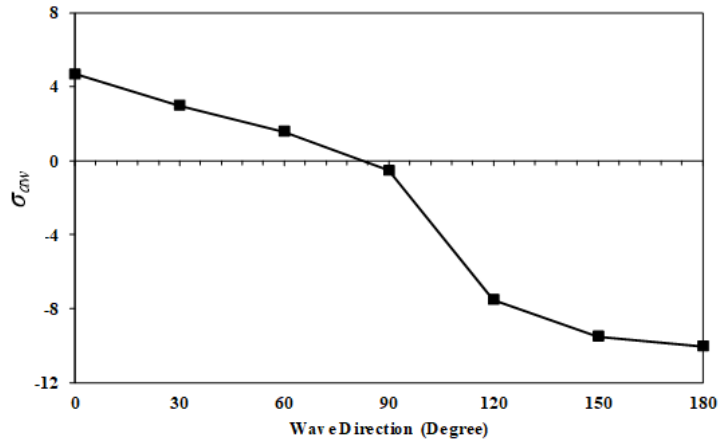

Figure 19. Added resistance coefficient at different wave collision angles

Figure 18 shows that the total resistance coefficient at different collision angles of the waves 0°, 30°, 60°, 90°, 120°, 150°, and 180°, respectively, are 0.004649, 0.002373, 0.001595, -0.00043, -0.00166, 0.00264 and -0.00425, while Figure 19 shows the additional resistance coefficient at different collision angles in the direction of 4.68810947 and 2.98334239, 1.56270316, -0.52043608, -7.52938794, -9.51828287, -10.0450559. Figure 18 shows that the total resistance coefficient varies depending on the wave angle. It is highest when waves strike the ship head-on (0 degrees) and decreases as the collision angle increases. Notably, the resistance coefficient becomes negative at certain angles, indicating that the wave interaction can reduce the ship's overall resistance. Figure 19 explores the additional resistance caused by wave interaction deeper. Similar to the total resistance, the collision angle influences the additional resistance. It reaches its

maximum values when waves approach the opposite direction (180 degrees) and tends towards zero when waves hit the ship from the side (90 degrees). Figure 19 suggests waves impacting the stern (angles exceeding 90 degrees) can generate negative additional resistance, effectively aiding the ship's movement. However, it is crucial to note that waves impacting the stern can be highly dangerous situations despite potentially reducing resistance. Such interactions can lead to "broaching," where the ship loses control and turns sideways to the waves, and "butterflies," where the bow lifts excessively out of the water.

4. CONCLUSIONS

The study reveals significant variations in container ship behavior due to changes in speed (Froude numbers) and wave impact angles. Numerical simulations using the k-ε turbulence model and Reynolds-Averaged Navier-Stokes equations demonstrated increased dynamic movements and additional resistance as the Froude number rises. Analyzing seven wave collision angles (0°-180°) for vertical and torsional motions, the research found that head-on wave impacts result in the maximum additional resistance. Maximum additional resistance occurred when waves impacted the ship head-on at 0°. The study revealed a correlation between increasing Froude number (ship speed) and two key factors affecting resistance: wetted surface area and wave breaking angle at the stern. The ship interacts more extensively with waves as speed increases, leading to a larger wetted surface area. Additionally, the results suggest a decrease in the wave-breaking angle at the stern. Both factors can directly contribute to higher resistance experienced by the ship. The results show a decrease in the wave refraction angle at the vessel's stern with increasing Froude number and increasing the Froude number, which translates to higher ship speeds and significantly amplifies both torsional and vertical motions. The study demonstrates that vertical motion is most significant when waves approach from a specific angle, i.e. 150°. Similarly, roll motion peaks when waves strike the ship from the side (angle of 90°). This is likely because wave interaction exerts a strong twisting force on the ship, inducing roll. Finally, it is found that the torsional deflection is most prominent at a particular angle of 60° during wave collisions. This study focused on regular waves. Future studies can be extended to explore the potential benefits of implementing active control systems to adjust ship movements based on wave conditions, potentially reducing resistance and improving stability.

ACKNOWLEDGEMENTS

The author(s) received no financial support for this article's research, authorship, and/or publication.

CONFLICT OF INTEREST

The authors declare that they do not have any conflict of interest.

AUTHORS CONTRIBUTION

M. Mokhtari (Writing Original Draft; Supervision; Experimental framework; Data analysis)

S. James (Writing Original Draft; Experimental work; Data curation; Writing – original draft)

Z. Razaviyan (Writing Original Draft; Data analysis; Experimental work; Writing – review and editing)

M. Heidari (Writing Original Draft; Visualization; Formal Analysis; Data Curation)

S. Thangavel (Visualization; Formal Analysis; Writing Original Draft; Data Curation)

A. Kumar (Writing Original Draft; Writing Review and Editing; Visualization; Methodology; Data Curation)

AVAILABILITY OF DATA AND MATERIALS

The data supporting this study's findings are available on request from the corresponding author.

ETHICS STATEMENT

Not applicable

REFERENCES

[1] J. Journee, "Motions, resistance, and propulsion of a ship in regular head waves," *Technical Report*, Delft University of Technology, 1976.

[2] R. T. Schmitke, "Ship sway, roll, and yaw motions in oblique seas," in *SNAME Annual Meeting, Society of Naval Architects and Marine Engineers,* pp. 1-15, 1978.

[3] R. F. Beck, A. M. Reed, "Modern computational methods for ships in a seaway," *Transitions of the Society of Naval Architects and Marine Engineers*, vol. 109, pp. 1-51, 2001.

[4] J. N. Newman, "The theory of ship motions," *Advances in Applied Mechanics*, vol. 18, pp. 221–283, 1979.

[5] O. M. Faltinsen, R. Zhao, N. Umeda "Numerical predictions of ship motions at high forward speed," *Philosophical Transactions: Physical Sciences and Engineering*, vol. 334, no. 1634, pp. 241-252, 1991.

[6] V. Yasukawa, H. Bertram, "Rankine source methods for seakeeping problems," in *Jahrbuch Schiffbautechnische Gesellschaft,* pp. 411-425, 1996.

[7] H. Yasukawa, "Application of 3-D time domain panel method to ship seakeeping problems," in *24th Symposium on Naval Hydrodynamics*, pp. 376-392, 2003.

[8] C. D. Simonsen, J. F. Otzen, S. Joncquez, F. Stern, "EFD and CFD for KCS heaving and pitching in regular head waves," *Journal of Marine Science and Technology,* vol. 18, pp. 435-459, 2013.

[9] T. Tezdogan, A. Incecik, O. Turan, "Operability assessment of high-speed passenger ships based on human comfort criteria," *Ocean Engineering* vol. 89, pp. 32-52, 2014.

[10] P. M. Carrica, K. J. Paik, H. S. Hosseini, F. Stern, "URANS analysis of a broaching event in irregular quartering seas," *Journal of Marine Science and Technology,* vol. 13, pp. 395-407, 2008.

[11] T. Castiglione, F. Stern, S. Bova, M. Kandasamy, "Numerical investigation of the seakeeping behavior of a catamaran advancing in regular head waves," *Ocean Engineering*, vol. 38, no. 16, pp.1806-1822, 2011.

[12] S. Castiglione, T. Sadat-Hosseini, H. Stern, F. Bova, "CFD simulation for sea keeping of Delft catamaran in regular head and oblique waves," in *Proceedings of the 12th International Conference on Fast Sea Transportation*, Netherland, 2013.

[13] C. D Simonsen, F. Stern, "CFD simulation of KCS sailing in regular head waves," in *Proceedings from Gothenburg 2010—A Workshop on Numerical Ship Hydrodynamics, Gothenburg*, 2010.

[14] S. Enger, M. Peric, R. Peric, "Simulation of flow around KCS-hull," in *Proceedings from Gothenburg 2010—A Workshop on Numerical Ship Hydrodynamics, Gothenburg*, 2010.

[15] S. Kim, H.-H Lee, "Fully nonlinear seakeeping analysis based on CFD simulations," in *21st International Ocean and Polar Engineering Conference*, Hawaii, United States, pp. ISOPE-I, 2011.

[16] H. Maruo, "The excess resistance of a ship in rough seas," *International Shipbuilding Progress*, vol. 4, no. 35, pp. 337-345, 1957.

[17] T. R. Goodman, "Forces on a hovering slender body of revolution submerged under waves of moderate wavelength," *Technical Report*, New York, no. 63-02, pp. 525-549, 1962.

[18] J. N. Newman, "The drift force and moment on ships in waves," *Journal of Ship Research*, vol. 11, pp. 51–60, 1967.

[19] J. Gerritsma, W. Beukelmann, "Analysis of the resistance increase in waves of a fast cargo ship," *International Shipbuilding Progress*, vol. 19, no. 217, pp. 285–293, 1972.

[20] O. M. Faltinsen, K. J. Minsaas, N. Liapis, S. O. Skjørdal, "Prediction of resistance and propulsion of a ship in a seaway," in *Proceeding of 13th Symposium on Naval Hydrodynamics*, pp. 505–529, 1980.

[21] J. A. Pinkster, "Mean and low-frequency wave drifting forces on floating structures," *Ocean Engineering*, vol. 6 no. 6, pp. 593–615, 1979.

[22] T. Tezdogan, Y. K. Demirel, P. Kellett, M. Khorasanchi, A. Incecik, O. Turan, "Full-scale unsteady RANS CFD simulations of ship behaviour and performance in head seas due to slow steaming," *Ocean Engineering*, vol. 97, pp. 186-206, 2015.

[23] A. Que´rard, P. Temarel, S. R. Turnock, "Influence of viscous effects on the hydrodynamics of ship-like sections undergoing symmetric and anti-symmetric motions using RANS," in *International Conference on Offshore Mechanics and Arctic Engineering*, vol. 48227, pp. 683-692, 2008.

[24] CD-Adapco*, User guide STAR-CCM+ Version 9.0.2.* 2014.

[25] J. C. Date, S. R. Turnock, "A study into the techniques needed to accurately predict skin friction using RANS solvers with validation against Froude's historical flat plate experimental data," *Ship Science Reports,* no. 114, University of Southampton, United Kingdom, 1999.

[26] S. A. Alterskjær, R. Eggers, Y. Gao, Y. Kim, D. Trodden, S. Werner, et al., "Predicting the power saving of wind-powered ships," *ITTC Recommended Procedures and Guidelines*, Switzerland, 2024.

[27] Z. Shen, D. Wan, "RANS computations of added resistance and motions of a ship in head waves," *International Journal of Offshore and Polar Engineering,* vol. 23, no. 4, pp. 264-271, 2013.

[28] D. Matulja, M. Sportelli, C. Guedes Soares, J. Prpić-Oršić, "Estimation of added resistance of a ship in regular waves," *An International Journal of Naval Architecture and Ocean Engineering for Research and Development*, vol. 62, no. 3, pp. 259-264, 2011.

[29] Y. K. Prajapati, P. K. Gupta, A. Kumar, "Free surface undulation and air entrainment in a rectangular tank," *International Journal of Applied Engineering Research,* vol. 6, no. 4, pp. 409-419, 2011.

[30] H. Wang, R. Zhu, L. Zha, M. Gu, "Experimental and numerical investigation on the resistance characteristics of a high-speed planing catamaran in calm water," *Ocean Engineering*, vol. 258, p. 111837, 2022.

[31] M. K. Awasthi, N. Dutt, A. Kumar, S. Kumar, "Electrohydrodynamic capillary instability of Rivlin–Ericksen viscoelastic fluid film with mass and heat transfer," *Heat Transfer*, vol. 53, no. 1, pp. 115-133, 2024.

[32] M. K Awasthi, A. Kumar, N. Dutt, S. Singh, *Computational Fluid Flow and Heat Transfer: Advances, Design, Control & Applications*, 1st ed. United States: CRC Press, 2024.

[33] A. Kumar, Y. Gori, N. Dutt, Y. K. Singla, A. Maurya, *Advanced Computational Methods in Mechanical and Materials Engineering*, 1st ed. United States: Taylor & Francis, 2021

[34] P. N. Reddy, V. Verma, A. Kumar, M. Awasthi, "CFD simulation and thermal performance optimization of flow in a channel with multiple baffles," *Journal of Heat and Mass Transfer Research*, vol. 10, no. 2, pp. 257-268, 2023.

[35] A. O. Elaghbash, "A CFD study of the resistance behavior of a planing hull in restricted waterways," *Sustainable Marine Structures*, vol. 3, no. 1, pp. 32-55, 2021.

[36] S. Riyadi, K. Suastika, "Experimental and numerical study of high Froude-number resistance of ship utilizing a hull vane®: A case study of a hard-chine crew boat," *CFD Letters*, vol, 12, no. 2, pp. 95-105, 2020.

[37] S. Tavakoli, R. N. Bilandi, S. Mancini, F. D. Luca, A. Dashtimanesh, "Dynamic of a planing hull in regular waves: Comparison of experimental, numerical and mathematical methods," *Ocean Engineering*, vol. 217, p. 107959, 2020.